

GEOMETRIC ERROR EFFECTS ON MANIPULATORS' POSITIONING PRECISION: A GENERAL ANALYSIS AND EVALUATION METHOD

Henrique Simas

Raul Guenther Lab. of Applied Robotics, Department of Mechanical Engineering,
Federal University of Santa Catarina, Florianópolis, SC- Brazil - 88040-900
E: henrique.simas@ufsc.br

Raffaele Di Gregorio (*)

Department of Engineering, University of Ferrara
Via Saragat,1; 44100 FERRARA; Italy
T: +39-0532-974828, F: +39-0532-974870, E: rdigregorio@ing.unife.it

ABSTRACT

Manufacturing and assembly (geometric) errors affect the positioning precision of manipulators. In six-degrees-of-freedom (6-DOF) manipulators, geometric error effects can be compensated through suitable calibration procedures. This, in general, is not possible in lower-mobility manipulators. Thus, methods that evaluate such effects must be implemented at the design stage to determine both which workspace region is less affected by these errors and which dimensional tolerances must be assigned to match given positioning-precision requirements. In the literature, such evaluations are mainly tailored on particular architectures and the proposed techniques are difficult to extend. Here, a general discussion on how to take into account geometric error effects is presented together with a general method to solve this design problem. The proposed method can be applied to any non-overconstrained architecture. Eventually, as a case study, the method is applied to the analysis of the geometric error effects of the translational parallel manipulator Triflex-II.

Keywords: lower-mobility manipulators, positioning precision, geometric errors, dimensional tolerances.

1. INTRODUCTION

Geometric accuracy is crucial for manipulators designed to accomplish high precision tasks since geometric errors affect end effector's positioning precision [1]. It requires small dimensional tolerances and precise assembly procedures. Both these requirements bring to increase manufacturing costs.

In six-degrees-of-freedom (6-DOF) manipulators, geometric error effects can be compensated through suitable calibration procedures and/or control algorithms [2]; whereas, in less-than-six-DOF (lower-mobility) manipulators, this, in general, cannot be done [3]. Thus, identifying manipulator configurations where the positioning precision is higher, and which geometric parameters need small tolerances is a mandatory step to implement when designing lower-mobility manipulators.

Lower-mobility manipulators, when applicable, are appealing since they offer simplified architectures, higher speeds and require only a few actuators [4,5]. Overconstrained manipulators are a family of lower-mobility manipulators. Such manipulators require precise manufacturing to avoid jamming and, at the design stage, models that take into account both link flexibility and external loads to prevent jamming [30]. Jamming avoidance requirements are usually tighter than positioning-precision ones. Therefore, positioning-precision requirements are somehow implicitly satisfied in those manipulators and, anyway, the models developed to prevent jamming can be used to check that positioning-precision requirements are matched, too. Differently, non-overconstrained lower-mobility manipulators need specific analyses (see, for instance, [31]) to satisfy positioning precision requirements. Thus, techniques that allow the analysis of their positioning precision are necessary.

In the literature, the most commonly adopted criteria to relate errors both in the values of the actuated-joint variables and/or in the geometric parameters to the pose error of the end effector are based on the condition number of suitable Jacobian matrices [2,4,6–16].

Gosselin and Angeles [7] proposed the *Global Conditioning Index* (GCI) to assess the distribution over the whole workspace of the condition number of the Jacobian that maps the actuated-joint rates onto end effector's twists. GCI proved to be a good index for both serial and parallel robots. Then, Merlet [9] reviewed and discussed the application of some accuracy criteria to serial and/or parallel manipulators including GCI.

For parallel manipulators, error detection methods [11,15], classification of errors [8], performance indices for joints with clearances [12] as well as strategies to overcome the geometric-error effects have been proposed. Also, Di Gregorio and Parenti-Castelli [3] stated some simple conditions on the Jacobian matrices that allow the separation of compensatable and uncompensatable errors. Later, Liu et al. [1] proposed an analytic technique based on homogeneous transformations and screw theory to obtain the same separation.

Some of the proposed methods [12–14] are based on classical tools, such as Denavit-Hartenberg convention or screw theory among others. Such methods seek for the best of each tool such as the improvement of the numerical efficiency.

In general, the works presented in the literature either address specific accuracy problems or analyze specific architectures. Both these points of view make the proposed methods difficult to extend.

The work presented here tries to overcome this limitation through a formalization of the positioning-precision problem that refers to a general architecture, which can be particularized to any serial or non-overconstrained parallel manipulator. The proposed formalization brings to naturally delineate a technique for taking into account geometric error effects. Such technique is well framed into the design procedure, and makes it possible to select either which workspace region is less affected by geometric errors or which geometric constants must be carefully sized to reduce these effects. The presented technique is also exemplified by illustrating its application to a lower-mobility parallel manipulator.

This paper is organized as follows. Section 2 resumes some background concepts and presents the adopted notations. Section 3 illustrates the proposed technique; then, section 4 discusses how geometric errors can be included in a general model. Eventually, section 5 illustrates one case study and section 6 draws the conclusions.

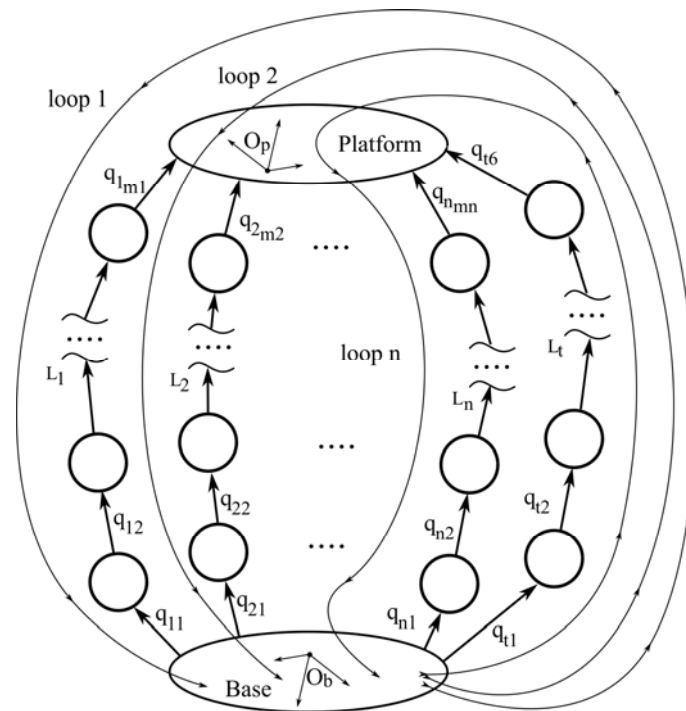


Figure 1: Graph of a manipulator with general architecture: vertices and arcs represent links and joints, respectively; L_i for $i=1, \dots, n$ are open kinematic chains (legs) which simultaneously connect the platform to the base; whereas, L_t is an added virtual kinematic chain.

2. BACKGROUND AND NOTATIONS

Figure 1 shows the graph [17,18] of a general manipulator architecture. In this graph, the vertices represent the links and the arcs represent the joints. The branches L_i , for $i=1,\dots,n$, are the open kinematic chains (legs) that simultaneously connect the end effector (platform) to the base in the manipulator (for serial manipulators $n=1$); whereas, the branch L_t is a virtual kinematic chain (VKC) which is added just to identify the platform pose through the values of its joint variables q_{ij} , for $j=1,\dots,6$. The joint variables of the i -th leg are denoted q_{ik} for $k=1,\dots,m_i$. $O_b-x_b y_b z_b$ and $O_p-x_p y_p z_p$ are two Cartesian reference systems fixed to base and platform, respectively. Since all the lower pairs can be transformed into suitable serial kinematic chain containing only revolute (R) and/or prismatic (P) pairs [19], all the joints are assumed to be R or P pairs without losing generality.

The general architecture of Fig. 1 has $(n-1)$ actual loops. Such loops contain a number, say r ($\equiv \sum_{i=1,n} m_i$), of joint variables that must satisfy the following relationship

$$r = f + d(n - 1) \quad (1)$$

where f is the DOF number of the manipulator, and d is the dimension of the displacement group the manipulator moves in (e.g., 3 for planar or spherical manipulators, 6 for spatial manipulators, etc. [20]). Hereafter, the set of joint variables will be split into f actuated-joint variables, collected into the f -tuple \mathbf{q}_f , and $(r-f)$ passive-joint variables, collected into the $(r-f)$ -tuple $\mathbf{q}_{(r-f)}$. Also, g and the g -tuple \mathbf{q}_g will denote the number of independent geometric constants that enter into the computation of the platform pose and the g -tuple that collects all these constants, respectively. Eventually, the 6-tuple \mathbf{q}_t will collect the six joint variables, q_{ij} for $j=1,\dots,6$, of the virtual kinematic chain L_t that parameterizes the platform pose

In order to take into account possible geometric errors, the manipulator must be always considered a spatial manipulator since, in general, geometric errors change the displacement group the manipulator moves in¹. As a consequence, the i -th loop, $i=1,\dots,n$, of Fig.1, constituted by the i -th branch L_i plus the VKC L_t , must be considered one spatial loop when writing the closure equations. In so doing, 6 independent scalar equations for each loop come out and the resulting closure equation system consists of $6n$ scalar equations, which contain all

¹ In lower-mobility manipulators (i.e., those with $f < 6$), the effects of the geometric errors that do not change the displacement group the platform moves in can generally be eliminated through calibration procedures [3].

the joint variables and the pose parameters of the platform. Such system can be written in vector form as follows:

$$\mathbf{F}(\mathbf{q}_t, \mathbf{q}_f, \mathbf{q}_{(r-f)}, \mathbf{q}_g) = \mathbf{0} \quad (2)$$

where $\mathbf{0}$ is the null vector, and \mathbf{F} is the (6n)-tuple that collects all the left-hand sides of the 6n scalar equations.

Equation (2) yields the following system of constraint equations in differential form

$$\mathbf{J}_t d\mathbf{q}_t = \mathbf{J}_f d\mathbf{q}_f + \mathbf{J}_{(r-f)} d\mathbf{q}_{(r-f)} + \mathbf{J}_g d\mathbf{q}_g \quad (3)$$

where \mathbf{J}_t , \mathbf{J}_f , $\mathbf{J}_{(r-f)}$, and \mathbf{J}_g are Jacobian matrices with 6n rows and respectively 6, f, (r-f) and g columns analytically defined as follows

$$\mathbf{J}_t = -\frac{d\mathbf{F}}{d\mathbf{q}_t}; \quad \mathbf{J}_f = \frac{d\mathbf{F}}{d\mathbf{q}_f}; \quad \mathbf{J}_{(r-f)} = \frac{d\mathbf{F}}{d\mathbf{q}_{(r-f)}}; \quad \mathbf{J}_g = \frac{d\mathbf{F}}{d\mathbf{q}_g} \quad (4)$$

The hypothesis, commonly adopted (1st order approximation), that the joint-variable errors $\Delta\mathbf{q}_f$ and $\Delta\mathbf{q}_{(r-f)}$, the geometric errors $\Delta\mathbf{q}_g$, and the errors $\Delta\mathbf{q}_t$, which must be used for computing the pose error of the platform, can replace the corresponding differentials into Eq. 3, yields the following relationship

$$\mathbf{J}_t \Delta\mathbf{q}_t = \mathbf{J}_f \Delta\mathbf{q}_f + \mathbf{J}_{(r-f)} \Delta\mathbf{q}_{(r-f)} + \mathbf{J}_g \Delta\mathbf{q}_g \quad (5)$$

3. EVALUATION OF GEOMETRIC ERROR EFFECTS

The set of independent geometric constants, which enter into the computation of the platform pose (i.e., the ones collected in \mathbf{q}_g), are either lengths or angles. Such lengths and angles can be considered the values assumed by the joint variables of locked P and R pairs, respectively, embedded in the links. By unlocking these P and R pairs, the actual manipulator generates an extended spatial mechanism (ESM) where the links of the actual manipulator are replaced by suitable kinematic chains and the \mathbf{q}_g entries are additional passive-joint variables. In the ESM, Eq. (3) become the analytic relationship among joint rates when rewritten as follows

$$\mathbf{J}_t \dot{\mathbf{q}}_t = \mathbf{J}_f \dot{\mathbf{q}}_f + \mathbf{J}_{(r-f)} \dot{\mathbf{q}}_{(r-f)} + \mathbf{J}_g \dot{\mathbf{q}}_g \quad (6)$$

Consequently, the ESM can be used to geometrically deduce the explicit expressions of all the above-defined Jacobian matrices by using screws [19].

Let $\boldsymbol{\omega}$ and \mathbf{v} denote respectively the angular velocity of the platform and the velocity of the platform point O_p (see Fig. 1), the platform twist $\$ [\equiv(\boldsymbol{\omega}^T, \mathbf{v}^T)^T]$ can be written in n different ways. Indeed, by moving from the base to the platform through the n legs L_i , $i=1, \dots, n$, of the ESM obtained from the corresponding legs of the actual manipulator (Fig.1), the following system of 6-dimensional vector equations comes out

$$\$ = \sum_{k=1, m_i} \hat{\$}_{ik} \dot{q}_{ik} + \sum_{p=1, g} \hat{\$}_p^i \dot{q}_p, \quad i=1, \dots, n \quad (7)$$

where q_p , for $p=1, \dots, g$, is the p -th entry of \mathbf{q}_g , and $\hat{\$}_{ik}$ is the unit screw² of the joint corresponding to the joint variable q_{ik} . Differently, $\hat{\$}_p^i$, for $p=1, \dots, g$, is equal to the unit screw of the joint corresponding to the joint variable q_p , if this joint belongs to the leg L_i , otherwise, it is a 6-dimensional null vector. The comparison of the right-hand sides of systems (6) and (7) straightforwardly yields the explicit expressions of the Jacobian matrices \mathbf{J}_f , $\mathbf{J}_{(r-f)}$, and \mathbf{J}_g .

3.1 Relationship between Pose Errors and Geometric Errors

The subtraction of the first vector equation of system (7) from the remaining $(n-1)$ transforms it as follows:

$$\$ = \sum_{k=1, m_1} \hat{\$}_{1k} \dot{q}_{1k} + \sum_{p=1, g} \hat{\$}_p^1 \dot{q}_p \quad (8a)$$

$$\mathbf{0} = \sum_{k=1, m_i} \hat{\$}_{ik} \dot{q}_{ik} - \sum_{k=1, m_1} \hat{\$}_{1k} \dot{q}_{1k} + \sum_{p=1, g} (\hat{\$}_p^i - \hat{\$}_p^1) \dot{q}_p, \quad i=2, \dots, n \quad (8b)$$

² Here, unit screws [19] are always equal to $(\mathbf{0}^T, \mathbf{s}^T)^T$ or $(\mathbf{s}^T, [(\mathbf{Q}-\mathbf{O}_p) \times \mathbf{s}]^T)^T$ respectively for P or R pairs, where \mathbf{s} and \mathbf{Q} are a unit vector parallel to the joint axis and a point of the same axis, respectively.

The introduction into Eqs. (8a) and (8b) of null 6-dimensional vectors that multiply the entries of $\dot{\mathbf{q}}_f$ and $\dot{\mathbf{q}}_{(r-f)}$, which do not appear at their right-hand sides, makes it possible to put system (8) in the following matrix form

$$\mathbf{\$} = \mathbf{A}_f \dot{\mathbf{q}}_f + \mathbf{A}_{(r-f)} \dot{\mathbf{q}}_{(r-f)} + \mathbf{A}_g \dot{\mathbf{q}}_g \quad (9a)$$

$$\mathbf{B}_{(r-f)} \dot{\mathbf{q}}_{(r-f)} = \mathbf{B}_f \dot{\mathbf{q}}_f + \mathbf{B}_g \dot{\mathbf{q}}_g \quad (9b)$$

where \mathbf{A}_f , $\mathbf{A}_{(r-f)}$, and \mathbf{A}_g are Jacobian matrices with 6 rows and respectively f , $(r-f)$ and g columns; whereas, \mathbf{B}_f , $\mathbf{B}_{(r-f)}$, and \mathbf{B}_g are Jacobian matrices with $6(n-1)$ rows and respectively f , $(r-f)$ and g columns.

Since linear system (9b) contains $6(n-1)$ scalar equations and, according to Eq. (1), the passive-joint variables (i.e., the entries of $\mathbf{q}_{(r-f)}$) are $d(n-1)$ with $d \leq 6$, $d(n-1)$ scalar equations of system (9b) can be always exploited to write the explicit expression of $\dot{\mathbf{q}}_{(r-f)}$ as follows

$$\dot{\mathbf{q}}_{(r-f)} = \mathbf{C}_f \dot{\mathbf{q}}_f + \mathbf{C}_g \dot{\mathbf{q}}_g \quad (10)$$

where \mathbf{C}_f , and \mathbf{C}_g are Jacobian matrices with $d(n-1)$ rows and respectively f and g columns.

The introduction of Eq. (10) into Eq. (9a) yields

$$\boldsymbol{\omega} = \mathbf{D}_f \dot{\mathbf{q}}_f + \mathbf{D}_g \dot{\mathbf{q}}_g \quad (11a)$$

$$\mathbf{v} = \mathbf{E}_f \dot{\mathbf{q}}_f + \mathbf{E}_g \dot{\mathbf{q}}_g \quad (11b)$$

where \mathbf{D}_f (\mathbf{E}_f), and \mathbf{D}_g (\mathbf{E}_g) are Jacobian matrices with 3 rows and respectively f and g columns defined as follows:

$$\begin{bmatrix} \mathbf{D}_f \\ \mathbf{E}_f \end{bmatrix} = \mathbf{A}_f + \mathbf{A}_{(r-f)} \mathbf{C}_f ; \quad \begin{bmatrix} \mathbf{D}_g \\ \mathbf{E}_g \end{bmatrix} = \mathbf{A}_g + \mathbf{A}_{(r-f)} \mathbf{C}_g \quad (12)$$

The above-mentioned 1st order approximation applied to Eqs. (11a) and (11b) yields

$$\mathbf{u}\Delta\varphi = \mathbf{D}_f \Delta\mathbf{q}_f + \mathbf{D}_g \Delta\mathbf{q}_g \quad (13a)$$

$$\Delta\mathbf{O}_p = \mathbf{E}_f \Delta\mathbf{q}_f + \mathbf{E}_g \Delta\mathbf{q}_g \quad (13b)$$

where $\Delta\mathbf{O}_p$ is the displacement of the platform point O_p (see Fig.1) due to the pose error and it measures platform's position error; whereas, \mathbf{u} and $\Delta\varphi$ are rotation-axis' unit vector and rotation angle, respectively, of the rotation matrix, say ${}^n\mathbf{R}_a$, that represents the rotation which makes the nominal platform orientation coincide with the actual one (i.e., the one that takes into account the orientation error of the platform).

It is worth noting that the 1st order approximation of ${}^n\mathbf{R}_a$ brings to write

$${}^n\mathbf{R}_a = \mathbf{I} + \mathbf{u}^{\text{Sk}} \Delta\varphi \quad (14)$$

where \mathbf{I} is the identity matrix and the right superscript "Sk" on a vector denotes the skew symmetric matrix associated to that vector.

3.2 Maximum Pose-Error Computation

Any definition of a vector norm induces the definition of a matrix norm, named operator norm, through the following relationship

$$\|\mathbf{A}\| = \max_{\mathbf{x} \neq \mathbf{0}} \frac{\|\mathbf{A}\mathbf{x}\|}{\|\mathbf{x}\|}, \quad (15)$$

Hereafter, the Euclidean norm for vectors and the induced operator norm (i.e., the spectral norm) for matrices³ will be used [21].

The triangle inequality of vector norms [21] applied to vector Eqs. (13a) and (13b) yields

$$|\Delta\varphi| \leq \|\mathbf{D}_f \Delta\mathbf{q}_f\| + \|\mathbf{D}_g \Delta\mathbf{q}_g\| \quad (16a)$$

$$\|\Delta\mathbf{O}_p\| \leq \|\mathbf{E}_f \Delta\mathbf{q}_f\| + \|\mathbf{E}_g \Delta\mathbf{q}_g\| \quad (16b)$$

³ The spectral norm of a real matrix \mathbf{A} is the square root of the largest eigenvalue of the positive-semidefinite matrix $\mathbf{A}^T \mathbf{A}$. The square roots of the eigenvalues of $\mathbf{A}^T \mathbf{A}$ are the "singular values" of \mathbf{A} ; thus, the spectral norm of \mathbf{A} is equal to its largest singular value.

Also, the application of the same norm property to each term at the right-hand sides of inequalities (16a) and (16b) yields

$$\|\mathbf{D}_f \Delta \mathbf{q}_f\| \leq \|\mathbf{D}_{f,P} \Delta \mathbf{q}_{f,P}\| + \|\mathbf{D}_{f,R} \Delta \mathbf{q}_{f,R}\| \quad (17a)$$

$$\|\mathbf{D}_g \Delta \mathbf{q}_g\| \leq \|\mathbf{D}_{g,P} \Delta \mathbf{q}_{g,P}\| + \|\mathbf{D}_{g,R} \Delta \mathbf{q}_{g,R}\| \quad (17b)$$

$$\|\mathbf{E}_f \Delta \mathbf{q}_f\| \leq \|\mathbf{E}_{f,P} \Delta \mathbf{q}_{f,P}\| + \|\mathbf{E}_{f,R} \Delta \mathbf{q}_{f,R}\| \quad (17c)$$

$$\|\mathbf{E}_g \Delta \mathbf{q}_g\| \leq \|\mathbf{E}_{g,P} \Delta \mathbf{q}_{g,P}\| + \|\mathbf{E}_{g,R} \Delta \mathbf{q}_{g,R}\| \quad (17d)$$

where $\mathbf{q}_{f,P}$ and $\mathbf{q}_{f,R}$ ($\mathbf{q}_{g,P}$ and $\mathbf{q}_{g,R}$) collect all the joint variables of P and R pairs, respectively, that appears in \mathbf{q}_f (in \mathbf{q}_g). $\mathbf{D}_{f,P}$ ($\mathbf{D}_{g,P}$) and $\mathbf{D}_{f,R}$ ($\mathbf{D}_{g,R}$) are Jacobian matrices which collect the columns of \mathbf{D}_f (\mathbf{D}_g) that refer to the entries of $\mathbf{q}_{f,P}$ and $\mathbf{q}_{f,R}$ (of $\mathbf{q}_{g,P}$ and $\mathbf{q}_{g,R}$), respectively. Analogously, $\mathbf{E}_{f,P}$ ($\mathbf{E}_{g,P}$) and $\mathbf{E}_{f,R}$ ($\mathbf{E}_{g,R}$) are Jacobian matrices which collect the columns of \mathbf{E}_f (\mathbf{E}_g) that refer to the entries of $\mathbf{q}_{f,P}$ and $\mathbf{q}_{f,R}$ (of $\mathbf{q}_{g,P}$ and $\mathbf{q}_{g,R}$), respectively. The entries of $\mathbf{q}_{f,P}$ and $\mathbf{q}_{g,P}$ ($\mathbf{q}_{f,R}$ and $\mathbf{q}_{g,R}$) are all lengths (angles); thus, $\mathbf{q}_{f,P}$ and $\mathbf{q}_{g,P}$ ($\mathbf{q}_{f,R}$ and $\mathbf{q}_{g,R}$) are homogeneous vectors and their Euclidean norm is dimensionally consistent.

By taking into account formulas (15) and (17) into inequalities (16a) and (16b), inequalities (16a) and (16b) are transformed as follows

$$|\Delta \varphi| \leq \delta_{f,P} \|\Delta \mathbf{q}_{f,P}\| + \delta_{f,R} \|\Delta \mathbf{q}_{f,R}\| + \delta_{g,P} \|\Delta \mathbf{q}_{g,P}\| + \delta_{g,R} \|\Delta \mathbf{q}_{g,R}\| \quad (18a)$$

$$\|\Delta \mathbf{O}_p\| \leq \varepsilon_{f,P} \|\Delta \mathbf{q}_{f,P}\| + \varepsilon_{f,R} \|\Delta \mathbf{q}_{f,R}\| + \varepsilon_{g,P} \|\Delta \mathbf{q}_{g,P}\| + \varepsilon_{g,R} \|\Delta \mathbf{q}_{g,R}\| \quad (18b)$$

where $\delta_{f,P}$, $\delta_{f,R}$, $\delta_{g,P}$, $\delta_{g,R}$, $\varepsilon_{f,P}$, $\varepsilon_{f,R}$, $\varepsilon_{g,P}$, and $\varepsilon_{g,R}$, hereafter referred to as “*accuracy coefficients*”, are the largest singular values of the Jacobian matrices $\mathbf{D}_{f,P}$, $\mathbf{D}_{f,R}$, $\mathbf{D}_{g,P}$, $\mathbf{D}_{g,R}$, $\mathbf{E}_{f,P}$, $\mathbf{E}_{f,R}$, $\mathbf{E}_{g,P}$, and $\mathbf{E}_{g,R}$, respectively.

Inequalities (18a) and (18b) highlight that the accuracy coefficients bound the effects on the pose errors both of the joint-variable errors and of the geometric errors. Thus, they can be used to quantify the local pose accuracy (LPA) of a manipulator. Actually, these coefficients depend on the manipulator configuration and can be mapped as a function of \mathbf{q}_f in the manipulator workspace. Accordingly, the global pose accuracy (GPA) can be measured by their average values on the useful workspace.

4. DISCUSSION

Since inequalities (18a) and (18b) hold, the design requirements $|\Delta\varphi| \leq |\Delta\varphi|_{\max}$ and $\|\Delta\mathbf{O}_p\| \leq \|\Delta\mathbf{O}_p\|_{\max}$, for assigned maximum values $|\Delta\varphi|_{\max}$ and $\|\Delta\mathbf{O}_p\|_{\max}$, are matched in the workspace regions where the following inequalities are satisfied

$$\delta_{f,P} \|\Delta\mathbf{q}_{f,P}\| + \delta_{f,R} \|\Delta\mathbf{q}_{f,R}\| + \delta_{g,P} \|\Delta\mathbf{q}_{g,P}\| + \delta_{g,R} \|\Delta\mathbf{q}_{g,R}\| \leq |\Delta\varphi|_{\max} \quad (19a)$$

$$\varepsilon_{f,P} \|\Delta\mathbf{q}_{f,P}\| + \varepsilon_{f,R} \|\Delta\mathbf{q}_{f,R}\| + \varepsilon_{g,P} \|\Delta\mathbf{q}_{g,P}\| + \varepsilon_{g,R} \|\Delta\mathbf{q}_{g,R}\| \leq \|\Delta\mathbf{O}_p\|_{\max} \quad (19b)$$

In order to satisfy conditions (19a) and (19b), designers can implement one or more of the following actions

a) *Dimensional synthesis*: the values of the accuracy coefficients can be reduced by suitably changing the sizes of the links,

b) *Control design*: the values of $\|\Delta\mathbf{q}_{f,P}\|$ and/or $\|\Delta\mathbf{q}_{f,R}\|$ can be reduced by improving actuators' hardware and/or the algorithms adopted to control the actuated-joint variables,

c) *Manufacturing precision*: the values of $\|\Delta\mathbf{q}_{g,P}\|$ and/or $\|\Delta\mathbf{q}_{g,R}\|$ can be reduced by reducing the dimensional tolerances on the link sizes.

The actions (b) and (c) can be further detailed until to determine the actuation or geometric tolerance of each entry of \mathbf{q}_f or \mathbf{q}_g . Indeed, the terms at the right-hand sides of inequalities (17a)–(17d) can be further partitioned until to contain only one \mathbf{q}_f or \mathbf{q}_g entry and the corresponding Jacobian matrix column. In so doing, the proposed method brings to conclude that the accuracy coefficient of a given entry of \mathbf{q}_f or \mathbf{q}_g is the square root of the dot product of the corresponding Jacobian-matrix column by itself (i.e., the magnitude of this column vector).

The actual use of the above-deduced formulas needs the identification of the set of independent geometric constants that enter into the platform-pose computation (i.e., the entries of \mathbf{q}_g). This apparently difficult task can be accomplished in many ways, for instance, by analyzing with a case-by-case approach the geometric constants that appear in the closure equation system. If a program that holds for any manipulator has to be developed, then the use of a standard convention [e.g., Denavit-Hartenberg (D-H) convention] that parameterizes both links' and joints' geometry becomes mandatory. In this case, the use of the D-H convention brings to introduce three geometric constants for each binary link.

In the literature (see, for instance, Refs. [6,7,9]), the effects of joint-variable errors are related to the “distance” of the manipulator configuration from the singular configurations [22–24]. Such “distance” is

evaluated with the “Conditioning Index” (CI). In serial (parallel) manipulators, the CI is defined as the inverse of the condition number of the Jacobian matrix whose product by the vector of the actuated-joint rates (the platform twist) yields the platform twist (the vector of the actuated-joint rates). It ranges from 0, at singular configurations, to 1, at isotropic configurations, which are the best configurations. If the spectral norm is adopted, the so-defined CI is equal to the ratio between the smallest and the largest singular values of the involved Jacobian matrix. If the involved Jacobian is interpreted as coefficient matrix of a linear input-output relationship, bounding its condition number corresponds to bounding the ratio (i.e., the gain) between the relative errors in the outputs and in the inputs [6,9].

The approaches based on the CI have a number of drawbacks (homogeneity of the involved inputs and outputs, meaningfulness of relative error for angular variables and poses, etc.) which can be somehow overcome, but they are not able to provide the tolerances on the actuation system in a straight way as the formulation proposed here does. Also, the formulation proposed here keeps the manipulator far from the singularities of the “Forward Instantaneous Kinematic Problem (FIKP)” [24] by bounding the largest singular values [see inequalities (19a) and (19b)], even though it does not provide a “distance” from such singularities. Nevertheless, it does not bound the “distance” from the singularities of the “Inverse Instantaneous Kinematic Problem (IIKP)” [24]. Such singularities are the configurations where the smallest singular values are equal to zero and are located at the workspace boundaries. Thus, bounding the minimum values of the smallest singular values is sufficient to keep the manipulator far from its workspace boundaries. Anyway, the minimum values to use depend on statics considerations⁴ and their determination is out of the scope of this paper.

5. CASE STUDY

Figure 2(a) shows a translational parallel manipulator (TPM) of type $\underline{P}RRR-\underline{P}RRU-\underline{P}RRS^5$, named Triflex-II [25]. Triflex-II is a patented 3-DOF non-overconstrained TPM, which came out as an evolution of Triflex-I [26,27] and Tripteron [28,29]. It features three legs connected to the base through three actuated prismatic pairs whose sliding directions are mutually orthogonal. In each leg, the sliding direction of the actuated P-pair and the axes of the R-pairs are all parallel. Also, in the U-joint, the R-pair axis fixed to the platform passes through the S-pair center, point A_2 of Fig. 2(b), and the other R-pair axis is parallel to the sliding direction of the P-pair of the $\underline{P}RRU$ leg.

⁴ It is worth reminding that, at the workspace boundaries, the platform pose does not change (along the directions perpendicular to the workspace boundaries) for an infinitesimal change of the actuated-joint variables [22,24], that is, in the 1st order approximation, the platform pose is insensible to actuated-joint variables' errors.

The length, a_p , of segment A_3O_p (see Fig. 2) is the minimum distance between the line passing through the U-joint center, point A_1 of Fig. 2(b), and the S-pair center, point A_2 , and the axis of the R-pair that joins the platform to the $\underline{P}RRR$ leg. The reference system $O_p-x_p y_p z_p$, fixed to the platform, has the y_p -axis coincident with the line passing through points A_1 and A_2 and the x_p -axis passing through point A_3 [Fig. 2(b)]. Hereafter, \mathbf{i}_p , \mathbf{j}_p , and \mathbf{k}_p denote the unit vectors of the coordinate axes x_p , y_p , and z_p , respectively.

The axes of the two cylindrical pairs (C-pairs) constituted by the $\underline{P}R$ chains that joins the $\underline{P}RRR$ and the $\underline{P}RRS$ legs intersect each other at O_b . [see Fig. 2(a)]. The reference system $O_b-x_b y_b z_b$, fixed to the base, has the z_b -axis (y_b -axis) coincident with the axis of the C-pair that joins the $\underline{P}RRR$ leg ($\underline{P}RRS$ leg) to the base. Hereafter, \mathbf{i}_b , \mathbf{j}_b , and \mathbf{k}_b denote the unit vectors of the coordinate axes x_b , y_b , and z_b , respectively.

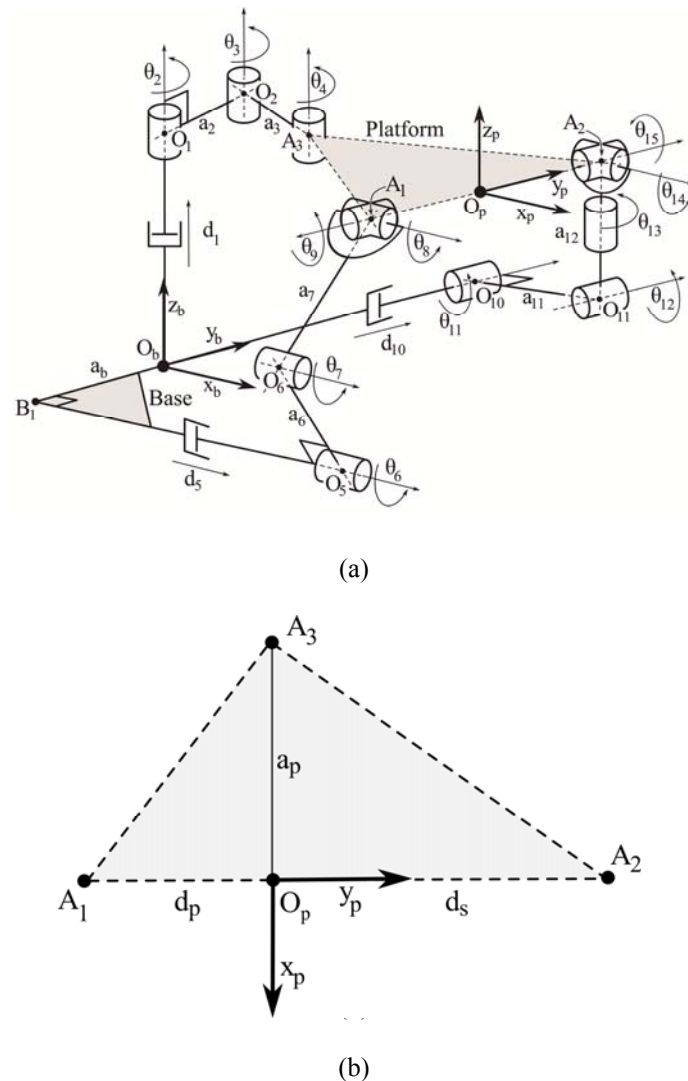


Figure 2: Triflex-II: (a) kinematic scheme, and (b) platform's reference points.

⁵ U and S stand for universal joint and spherical pair, respectively. The underscore indicates an actuated joint. The hyphen separates the strings that give legs' topology by moving from the base to the platform (Fig.1).

Also, with reference to the points indicated in Fig. 2, the following segment lengths are defined. In the base, a_b is the constant length of segment O_bB_1 ; d_1 , d_5 , and d_{10} are the variable lengths of the segments O_bO_1 , B_1O_5 , and O_bO_{10} , respectively. In the platform, d_p and d_s are the constant lengths of the segments O_pA_1 and O_pA_2 , respectively. In the $\underline{P}RRR$ leg, a_2 and a_3 are the constant lengths of the segments O_1O_2 and O_2A_3 , respectively. In the $\underline{P}RRU$ leg, a_6 and a_7 are the constant lengths of the segments O_5O_6 and O_6A_1 , respectively. In the $\underline{P}RRS$ leg, a_{11} and a_{12} are the constant lengths of the segments $O_{10}O_{11}$ and $O_{11}A_2$, respectively. The three actuated-joint variables are d_1 , d_5 , and d_{10} , that is, $\mathbf{q}_f = (d_1, d_5, d_{10})^T$.

Eventually, in Fig. 2, the twelve angles $\theta_2, \theta_3, \theta_4, \theta_6, \theta_7, \theta_8, \theta_9, \theta_{11}, \theta_{12}, \theta_{13}, \theta_{14}$, and θ_{15} are the passive-joint variables, that is, $\mathbf{q}_{f-f} = (\theta_2, \theta_3, \theta_4, \theta_6, \theta_7, \theta_8, \theta_9, \theta_{11}, \theta_{12}, \theta_{13}, \theta_{14}, \theta_{15})^T$. These angles are defined according to the D-H convention.

5.1 Determination of the Independent Geometric Constants

Triflex-II is a spatial manipulator, which makes the platform translate with respect to the base. Its kinematic behavior is easy to understand when realizing that the $\underline{P}RRR$ leg constrains the platform to make a Shoeflies motion, which, here, is a planar motion whose motion plane is parallel to the $x_b y_b$ plane and can perform controlled translations along the z_b -axis. Then, the $\underline{P}RRU$ leg forbids the remaining platform rotation around the z_b -axis with its U-joint and controls the platform translation along the x_b -axis with its actuated P-pair; whereas, the $\underline{P}RRS$ leg uniquely controls the platform translation along y_b -axis with its actuated P-pair.

The effects of all the geometric errors that do not violate the translational nature of this TPM can be eliminated through calibration procedures [3]. Since calibration procedures are much cheaper than the manufacture of components with smaller dimensional tolerances, the geometric constants whose errors do not affect the translational constraint between platform and base are assumed without relevant geometric errors. Also, the links are all assumed rigid.

In the Triflex-II, the base geometry just fixes the angles among the three P-pair sliding directions. Since it is quite clear that the translational constraint between platform and base keeps valid, even though these three directions are not mutually orthogonal (provided they are not coplanar), the base geometry will be assumed without geometric errors.

The platform geometry fixes the minimum distance, a_p [Fig. 2(b)], between two R-pair axes (one of the $\underline{P}RRR$ leg and the other of the $\underline{P}RRU$ leg) and the mutual positions among these axes and the centers of the U-joint and of the S-pair. Since any variation in these geometric data just yields a constant change in the location of

the $O_p-x_p y_p z_p$ reference frame, which does not affect the translational constraint between platform and base, the platform geometry will be assumed without geometric errors.

Regarding the PRRS leg, a simple static analysis, which is immediately clear by using the screw theory, reveals that the wrench, this leg applies to the platform, is one force whose line of action passes through A_2 and is parallel to the sliding direction, \mathbf{j}_b , of the P-pair. Moreover, the same analysis highlights that this result does not depend on the parallelism of the R-pair axes and on the values of the lengths a_{11} and a_{12} . Since geometric errors in this leg do not affect its kinetostatic role and the translational constraint between platform and base, the PRRS leg will be assumed without geometric errors. The adopted notation (Fig. 2) makes it possible to write Eq. (7) of this leg as follows

$$\mathcal{S} = \hat{\mathcal{S}}_{10} \dot{d}_{10} + \sum_{k=1,5} \hat{\mathcal{S}}_{1k} \dot{\theta}_{1k} \quad (20)$$

where

$$\begin{aligned} \hat{\mathcal{S}}_{10} &= \begin{bmatrix} \mathbf{0} \\ \mathbf{j}_b \end{bmatrix}; \quad \hat{\mathcal{S}}_{11} = \begin{bmatrix} \mathbf{j}_b \\ (\mathbf{O}_{10} - \mathbf{O}_p) \times \mathbf{j}_b \end{bmatrix}; \quad \hat{\mathcal{S}}_{12} = \begin{bmatrix} \mathbf{j}_b \\ (\mathbf{O}_{11} - \mathbf{O}_p) \times \mathbf{j}_b \end{bmatrix}; \\ \hat{\mathcal{S}}_{13} &= \begin{bmatrix} \mathbf{i}_{12} \\ (\mathbf{A}_2 - \mathbf{O}_p) \times \mathbf{i}_{12} \end{bmatrix}; \quad \hat{\mathcal{S}}_{14} = \begin{bmatrix} \mathbf{i}_{13} \\ (\mathbf{A}_2 - \mathbf{O}_p) \times \mathbf{i}_{13} \end{bmatrix}; \quad \hat{\mathcal{S}}_{15} = \begin{bmatrix} \mathbf{j}_p \\ \mathbf{0} \end{bmatrix}; \end{aligned}$$

with

$$\mathbf{i}_{12} = \frac{(\mathbf{A}_2 - \mathbf{O}_{11})}{a_{12}}; \quad \mathbf{i}_{13} = \frac{\mathbf{i}_{12} \times \mathbf{j}_p}{\|\mathbf{i}_{12} \times \mathbf{j}_p\|}.$$

Regarding the PRRU leg, an analogous static analysis reveals that the wrench, this leg applies to the platform, is constituted by one force, whose line of action passes through A_1 and is parallel to the sliding direction, \mathbf{i}_b , of the P-pair, and one torque, perpendicular to the two R-pair axes of the U-joint. The same analysis highlights that this result does not depend on the parallelism of the R-pair axes and on the values of the lengths a_6 and a_7 . Even though PRRU leg's geometric errors do not affect its static role, a mobility analysis reveals that the translational constraint between platform and base needs the parallelism of the axes of the three intermediate R pairs, and the perpendicularity of the axes of the two R pairs that form the U joint. Therefore, it will be assumed that geometric errors are present only in the parallelism of the axes of the three intermediate R pairs, and in the perpendicularity of the axes of the two R pairs that form the U joint. In so doing, this leg geometry is modified as shown in Fig. 3(a) where d_6 , d_7 , α_6 , α_7 , and α_8 are the geometric errors.

With reference to Fig. 3(a), \mathbf{i}_6 and \mathbf{i}_7 are the unit vectors of the second and third R-pair axes, respectively, and the following relationships hold

$$\mathbf{i}_6 = \mathbf{i}_b \cos\alpha_6 + (\mathbf{u}_6 \times \mathbf{i}_b) \sin\alpha_6 \quad (21a)$$

$$\mathbf{i}_7 = \mathbf{i}_6 \cos\alpha_7 + (\mathbf{u}_7 \times \mathbf{i}_6) \sin\alpha_7 \quad (21b)$$

$$d_6 = (\mathbf{O}_6 - \mathbf{O}_{6'}) \cdot \mathbf{i}_6 \quad (21c)$$

$$d_7 = (\mathbf{A}_1 - \mathbf{O}_7) \cdot \mathbf{i}_7 \quad (21d)$$

where $\mathbf{u}_6 = (\mathbf{O}_6 - \mathbf{O}_5)/a_6$ and $\mathbf{u}_7 = (\mathbf{O}_7 - \mathbf{O}_6)/a_7$. In addition, Eq. (7) of this leg can be written as follows

$$\dot{\$} = \dot{\$}_5 \dot{d}_5 + \sum_{j=6,9} \dot{\$}_j \dot{\theta}_j + \sum_{k=6,7} (\dot{\$}_{P,k} \dot{d}_k + \dot{\$}_{R,k} \dot{\alpha}_k) + \dot{\$}_{R,8} \dot{\alpha}_8 \quad (22)$$

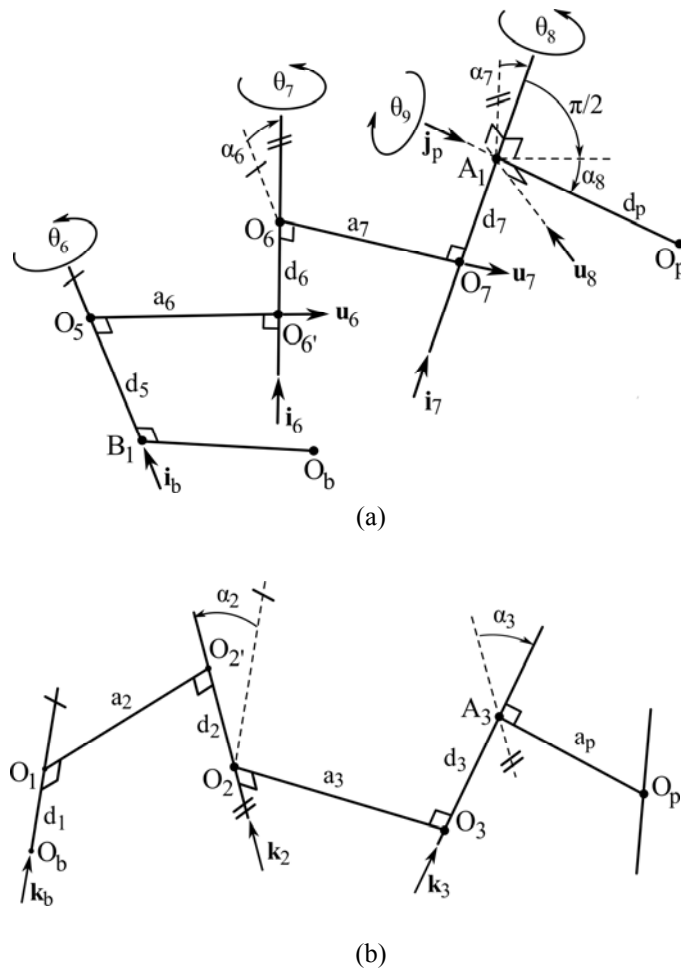


Figure 3: Introduction of the geometric errors: (a) PRRU and (b) PRRR legs with geometric errors.

where

$$\begin{aligned} \hat{\$}_5 &= \begin{bmatrix} \mathbf{0} \\ \mathbf{i}_b \end{bmatrix}; \hat{\$}_6 = \begin{bmatrix} \mathbf{i}_b \\ (\mathbf{O}_5 - \mathbf{O}_p) \times \mathbf{i}_b \end{bmatrix}; \hat{\$}_7 = \begin{bmatrix} \mathbf{i}_6 \\ (\mathbf{O}_6 - \mathbf{O}_p) \times \mathbf{i}_6 \end{bmatrix}; \hat{\$}_8 = \begin{bmatrix} \mathbf{i}_7 \\ (\mathbf{A}_1 - \mathbf{O}_p) \times \mathbf{i}_7 \end{bmatrix}; \\ \hat{\$}_9 &= \begin{bmatrix} \mathbf{j}_p \\ \mathbf{0} \end{bmatrix}; \hat{\$}_{p,6} = \begin{bmatrix} \mathbf{0} \\ \mathbf{i}_6 \end{bmatrix}; \hat{\$}_{p,7} = \begin{bmatrix} \mathbf{0} \\ \mathbf{i}_7 \end{bmatrix}; \hat{\$}_{R,6} = \begin{bmatrix} \mathbf{u}_6 \\ (\mathbf{O}_5 - \mathbf{O}_p) \times \mathbf{u}_6 \end{bmatrix}; \hat{\$}_{R,7} = \begin{bmatrix} \mathbf{u}_7 \\ (\mathbf{O}_6 - \mathbf{O}_p) \times \mathbf{u}_7 \end{bmatrix}; \hat{\$}_{R,8} = \begin{bmatrix} \mathbf{u}_8 \\ (\mathbf{A}_1 - \mathbf{O}_p) \times \mathbf{u}_8 \end{bmatrix}. \end{aligned}$$

with

$$\mathbf{u}_8 = \frac{\mathbf{i}_7 \times \mathbf{j}_p}{\|\mathbf{i}_7 \times \mathbf{j}_p\|}.$$

Regarding the PRRR leg, a possible error in the parallelism between P-pair's sliding direction and the axis of the first R-pair or in the values of the lengths a_2 and a_3 does not change the type of motion it imposes to the platform (i.e., it still is a Shoeflies motion). On the contrary, a possible error in the parallelism among the three R-pair axes do change that motion and violate the translational constraint between platform and base. Therefore, it will be assumed that geometric errors are present only in the parallelism among the three R-pair axes. In so doing, this leg geometry is modified as shown in Fig. 3(b) where d_2 , d_3 , α_2 and α_3 are the geometric errors.

With reference to Fig. 3(b), \mathbf{k}_2 and \mathbf{k}_3 are the unit vectors of the second and the third R-pair axes, respectively, and the following relationship hold

$$\mathbf{k}_2 = \mathbf{k}_b \cos\alpha_2 + (\mathbf{i}_2 \times \mathbf{k}_b) \sin\alpha_2 \quad (23a)$$

$$\mathbf{k}_3 = \mathbf{k}_2 \cos\alpha_3 + (\mathbf{i}_3 \times \mathbf{k}_2) \sin\alpha_3 \quad (23b)$$

$$d_2 = (\mathbf{O}_2 - \mathbf{O}_2') \cdot \mathbf{k}_2 \quad (23c)$$

$$d_3 = (\mathbf{A}_3 - \mathbf{O}_3) \cdot \mathbf{k}_3 \quad (23d)$$

where $\mathbf{i}_2 = (\mathbf{O}_2' - \mathbf{O}_1)/a_2$ and $\mathbf{i}_3 = (\mathbf{O}_3 - \mathbf{O}_2)/a_3$. Also, Equation (7) of the PRRR leg can be written as follows

$$\$\ = \hat{\$}_1 \dot{d}_1 + \sum_{j=2,4} \hat{\$}_j \dot{\theta}_j + \sum_{k=2,3} (\hat{\$}_{p,k} \dot{d}_k + \hat{\$}_{R,k} \dot{\alpha}_k) \quad (24)$$

where

$$\hat{\$}_1 = \begin{bmatrix} \mathbf{0} \\ \mathbf{k}_b \end{bmatrix}; \hat{\$}_2 = \begin{bmatrix} \mathbf{k}_b \\ (\mathbf{O}_1 - \mathbf{O}_p) \times \mathbf{k}_b \end{bmatrix}; \hat{\$}_3 = \begin{bmatrix} \mathbf{k}_2 \\ (\mathbf{O}_2 - \mathbf{O}_p) \times \mathbf{k}_2 \end{bmatrix}; \hat{\$}_4 = \begin{bmatrix} \mathbf{k}_3 \\ (\mathbf{A}_3 - \mathbf{O}_p) \times \mathbf{k}_3 \end{bmatrix};$$

$$\hat{\$}_{p,2} = \begin{bmatrix} \mathbf{0} \\ \mathbf{k}_2 \end{bmatrix}; \quad \hat{\$}_{p,3} = \begin{bmatrix} \mathbf{0} \\ \mathbf{k}_3 \end{bmatrix}; \quad \hat{\$}_{R,2} = \begin{bmatrix} \mathbf{i}_2 \\ (\mathbf{O}_1 - \mathbf{O}_p) \times \mathbf{i}_2 \end{bmatrix}; \quad \hat{\$}_{R,3} = \begin{bmatrix} \mathbf{i}_3 \\ (\mathbf{O}_2 - \mathbf{O}_p) \times \mathbf{i}_3 \end{bmatrix}.$$

The conclusion is that, in the Triflex-II, $\mathbf{q}_g = (d_2, d_3, d_6, d_7, \alpha_2, \alpha_3, \alpha_6, \alpha_7, \alpha_8)^T$ with $\mathbf{q}_{g,p} = (d_2, d_3, d_6, d_7)^T$ and $\mathbf{q}_{g,R} = (\alpha_2, \alpha_3, \alpha_6, \alpha_7, \alpha_8)^T$.

5.2 ESM and Jacobian Matrices

The analysis reported in sub-section 5.1 shows that the ESM of the Triflex-II is obtained from the nominal geometry of Fig. 2(a) by modifying the geometry of the $\underline{P}RRU$ and $\underline{P}RRR$ legs as shown in Fig.3 and by considering $d_2, d_3, d_6, d_7, \alpha_2, \alpha_3, \alpha_6, \alpha_7$ and α_8 as additional joint variables. Thus, the ESM is a $\underline{P}RRPRRPR$ - $\underline{P}RRPRRPRR$ - $\underline{P}RRS$ mechanism. Equations (20), (22) and (24) constitute system (7) of this ESM. If Eq. (24) is used as Eq. (8a) and it is subtracted from the remaining two equations, such system can be transformed as follows

$$\dot{\$} = \hat{\$}_1 \dot{d}_1 + \sum_{j=2,4} \hat{\$}_j \dot{\theta}_j + \sum_{k=2,3} (\hat{\$}_{p,k} \dot{d}_k + \hat{\$}_{R,k} \dot{\alpha}_k) \quad (25a)$$

$$\mathbf{0} = -\hat{\$}_1 \dot{d}_1 + \hat{\$}_{10} \dot{d}_{10} - \sum_{j=2,4} \hat{\$}_j \dot{\theta}_j + \sum_{i=1,5} \hat{\$}_{1i} \dot{\theta}_{1i} - \sum_{k=2,3} (\hat{\$}_{p,k} \dot{d}_k + \hat{\$}_{R,k} \dot{\alpha}_k) \quad (25b)$$

$$\mathbf{0} = -\hat{\$}_1 \dot{d}_1 + \hat{\$}_5 \dot{d}_5 - \sum_{j=2,4} \hat{\$}_j \dot{\theta}_j + \sum_{i=6,9} \hat{\$}_i \dot{\theta}_i - \sum_{k=2,3} (\hat{\$}_{p,k} \dot{d}_k + \hat{\$}_{R,k} \dot{\alpha}_k) + \sum_{k=6,7} (\hat{\$}_{p,k} \dot{d}_k + \hat{\$}_{R,k} \dot{\alpha}_k) + \hat{\$}_{R,8} \dot{\alpha}_8 \quad (25c)$$

System (25) can be put in the canonical form of system (9), that is,

$$\dot{\$} = \mathbf{A}_f \dot{\mathbf{q}}_f + \mathbf{A}_{(r-f)} \dot{\mathbf{q}}_{(r-f)} + \mathbf{A}_g \dot{\mathbf{q}}_g \quad (9a)$$

$$\mathbf{B}_{(r-f)} \dot{\mathbf{q}}_{(r-f)} = \mathbf{B}_f \dot{\mathbf{q}}_f + \mathbf{B}_g \dot{\mathbf{q}}_g, \quad (9b)$$

with the following definitions

$$\mathbf{A}_f = [\hat{\$}_1, \mathbf{0}, \mathbf{0}]; \quad \mathbf{A}_{r-f} = [\hat{\$}_2, \hat{\$}_3, \hat{\$}_4, \mathbf{0}, \mathbf{0}, \mathbf{0}, \mathbf{0}, \mathbf{0}, \mathbf{0}, \mathbf{0}, \mathbf{0}, \mathbf{0}]; \quad \mathbf{A}_g = [\hat{\$}_{p,2}, \hat{\$}_{p,3}, \mathbf{0}, \mathbf{0}, \hat{\$}_{R,2}, \hat{\$}_{R,3}, \mathbf{0}, \mathbf{0}, \mathbf{0}];$$

$$\mathbf{B}_f = \begin{bmatrix} -\hat{\$}_1 & \mathbf{0} & \hat{\$}_{10} \\ -\hat{\$}_1 & \hat{\$}_5 & \mathbf{0} \end{bmatrix}; \quad \mathbf{B}_g = - \begin{bmatrix} \hat{\$}_{p,2} & \hat{\$}_{p,3} & \mathbf{0} & \mathbf{0} & \hat{\$}_{R,2} & \hat{\$}_{R,3} & \mathbf{0} & \mathbf{0} & \mathbf{0} \\ \hat{\$}_{p,2} & \hat{\$}_{p,3} & -\hat{\$}_{p,6} & -\hat{\$}_{p,7} & \hat{\$}_{R,2} & \hat{\$}_{R,3} & -\hat{\$}_{R,6} & -\hat{\$}_{R,7} & -\hat{\$}_{R,8} \end{bmatrix};$$

$$\mathbf{B}_{f-f} = \begin{bmatrix} \hat{\$}_2 & \hat{\$}_3 & \hat{\$}_4 & \mathbf{0} & \mathbf{0} & \mathbf{0} & \mathbf{0} & -\hat{\$}_{11} & -\hat{\$}_{12} & -\hat{\$}_{13} & -\hat{\$}_{14} & -\hat{\$}_{15} \\ \hat{\$}_2 & \hat{\$}_3 & \hat{\$}_4 & -\hat{\$}_6 & -\hat{\$}_7 & -\hat{\$}_8 & -\hat{\$}_9 & \mathbf{0} & \mathbf{0} & \mathbf{0} & \mathbf{0} & \mathbf{0} \end{bmatrix};$$

$$\mathbf{q}_f = (d_1, d_5, d_{10})^T; \quad \mathbf{q}_g = (d_2, d_3, d_6, d_7, \alpha_2, \alpha_3, \alpha_6, \alpha_7, \alpha_8)^T;$$

$$\mathbf{q}_{f-f} = (\theta_2, \theta_3, \theta_4, \theta_6, \theta_7, \theta_8, \theta_9, \theta_{11}, \theta_{12}, \theta_{13}, \theta_{14}, \theta_{15})^T.$$

Also, in this case, the matrices \mathbf{C}_f and \mathbf{C}_g of system (10) are

$$\mathbf{C}_f = \mathbf{B}_{f-f}^{-1} \mathbf{B}_f, \quad \mathbf{C}_g = \mathbf{B}_{f-f}^{-1} \mathbf{B}_g.$$

5.3 Determination of the Accuracy Coefficients

In the nominal geometry [i.e., with reference to Figs. 3(a) and 3(b), when $\mathbf{k}_2=\mathbf{k}_3=\mathbf{k}_b$, $\mathbf{O}_2\equiv\mathbf{O}_2$, $\mathbf{O}_3\equiv\mathbf{A}_3$, $\mathbf{i}_6=\mathbf{i}_7=\mathbf{i}_b$, $\mathbf{O}_6\equiv\mathbf{O}_6$ and $\mathbf{O}_7\equiv\mathbf{A}_1$], \mathbf{D}_f is the 3×3 null matrix and \mathbf{E}_f is the 3×3 identity matrix (Triflex-II is a fully-isotropic TPM [25]). Also, $\mathbf{D}_{g,p}$ is the 3×4 null matrix and $\mathbf{E}_{g,p}$ is a 3×4 constant matrix equal to $[\mathbf{k}_b, \mathbf{k}_b, \mathbf{i}_b, \mathbf{i}_b]$; whereas, $\mathbf{D}_{g,R}$ and $\mathbf{E}_{g,R}$ are 3×5 configuration-dependent matrices respectively equal to $[\mathbf{i}_2, \mathbf{i}_3, \mathbf{v}_6, \mathbf{v}_7, \mathbf{k}_b]$ and to $[\mathbf{s}_2, \mathbf{s}_3, \mathbf{s}_6, \mathbf{s}_7, \mathbf{s}_8]$ with $\mathbf{v}_6 = (\mathbf{u}_6 \cdot \mathbf{k}_b) \mathbf{k}_b$, $\mathbf{v}_7 = (\mathbf{u}_7 \cdot \mathbf{k}_b) \mathbf{k}_b$, $\mathbf{s}_2 = (\mathbf{O}_1 - \mathbf{O}_p) \times \mathbf{i}_2$, $\mathbf{s}_3 = (\mathbf{O}_2 - \mathbf{O}_p) \times \mathbf{i}_3$, $\mathbf{s}_6 = (\mathbf{O}_5 - \mathbf{O}_p) \times \mathbf{u}_6$, $\mathbf{s}_7 = (\mathbf{O}_6 - \mathbf{O}_p) \times \mathbf{u}_7$ and $\mathbf{s}_8 = (\mathbf{A}_1 - \mathbf{O}_p) \times \mathbf{k}_b$. The result is that $\delta_{f,p}$, $\delta_{f,R}$, $\delta_{g,p}$, and $\varepsilon_{f,R}$ are all equal to zero, $\varepsilon_{f,p}$ and $\varepsilon_{g,p}$ are equal to 1 and $\sqrt{2}$, respectively, and inequalities (18a) and (18b) become

$$|\Delta\varphi| \leq \delta_{g,R} \|\Delta\mathbf{q}_{g,R}\| \quad (26a)$$

$$\|\Delta\mathbf{O}_p\| \leq \|\Delta\mathbf{q}_{f,p}\| + \sqrt{2} \|\Delta\mathbf{q}_{g,p}\| + \varepsilon_{g,R} \|\Delta\mathbf{q}_{g,R}\| \quad (26b)$$

where $\mathbf{q}_{f,p}$ coincides with \mathbf{q}_f , $\mathbf{q}_{g,p} = (d_2, d_3, d_6, d_7)^T$, $\mathbf{q}_{g,R} = (\alpha_2, \alpha_3, \alpha_6, \alpha_7, \alpha_8)^T$, and

$$\delta_{g,R} = \max \left\{ \sqrt{1 + |\mathbf{i}_2 \cdot \mathbf{i}_3|}, \sqrt{1 + |\mathbf{u}_6 \cdot \mathbf{u}_8|^2 + |\mathbf{u}_7 \cdot \mathbf{u}_8|^2} \right\} \quad (27a)$$

$$\varepsilon_{g,R} = \max \left\{ \sqrt{|\mathbf{s}_2|^2 + |\mathbf{s}_3|^2}, \sqrt{|\mathbf{s}_6|^2 + |\mathbf{s}_7|^2 + |\mathbf{s}_8|^2} \right\} \quad (27b)$$

The analysis of Fig. 2(a) and of Eq.(27)⁶ reveals that the maximum value of $\delta_{g,R}$ (i.e., $\delta_{g,R}=\sqrt{3}$) occurs when, in the PRRU leg, O_5 , O_6 and A_1 are aligned and orthogonal to the segment A_1O_p ; whereas, its minimum value (i.e., $\delta_{g,R}=1$) occurs when the two segment O_1O_2 and O_2A_3 are orthogonal in the PRRR leg and O_p , O_5 , O_6 , and A_1 are aligned in the PRRU leg. Also, the minimum value of $\varepsilon_{g,R}$ (i.e., $\varepsilon_{g,R}=d_p$) occurs when O_p , O_1 , O_2 , and A_3 are aligned in the PRRR leg and O_p , O_5 , O_6 , and A_1 are aligned in the PRRU leg.

The values of $\delta_{g,R}$ and $\varepsilon_{g,R}$ can be computed for each point of the workspace volume by using Eq. (27). Since Triflex-II is a TPM, the coordinates, $(x, y, z)^T$, of point O_p , measured in the reference system $O_b-x_b y_b z_b$, fixed to the base, uniquely identify the poses the platform can actually assume. Due to the three C-pairs that join the legs to the base, such O_p coordinates are bounded to stay inside the volume that is the common intersection among three right circular cylinders. The first one (due to the PRRR leg) has the axis parallel to the z_b axis and passing through the point $(a_p,0,0)^T$, and has the radius of the cross section equal to (a_2+a_3) . The second one (due to the PRRS leg) has the axis coincident with the y_b axis and the radius of the cross section equal to $(a_{11}+a_{12})$. The third one (due to the PRRU leg) has the axis parallel to the x_b axis and passing through the point $(0,d_p-a_b,0)^T$, and has the radius of the cross section equal to (a_6+a_7) . Since the poses, the platform can assume, are

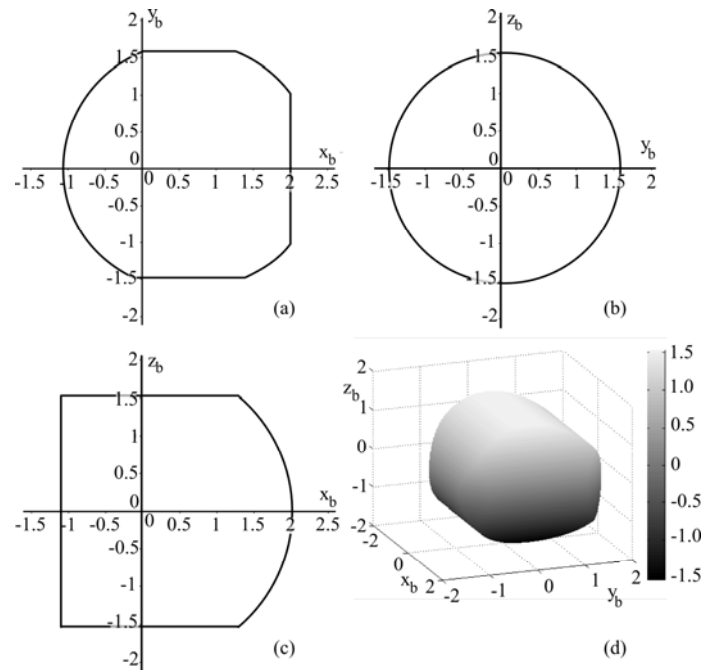
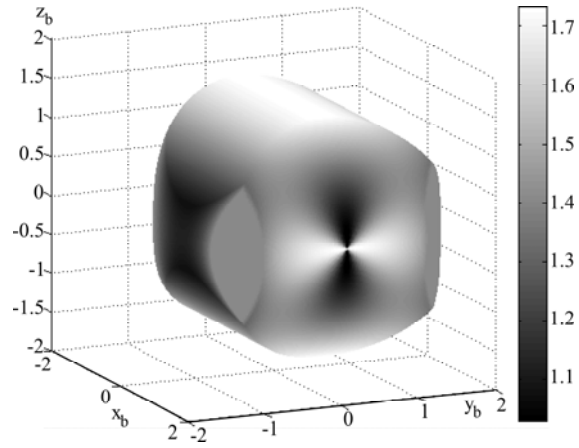
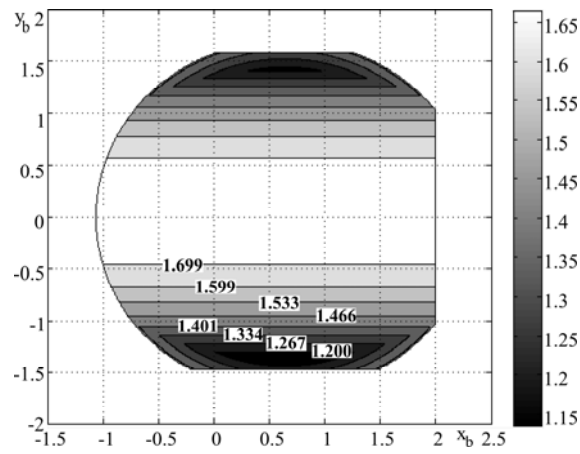


Figure 4: Workspace boundaries: (a) intersection with the $x_b y_b$ -plane, (b) intersection with the $y_b z_b$ -plane, (c) intersection with the $x_b z_b$ -plane, and (d) 3D view (the grayscale indicates the z_b value in [l.u.]).

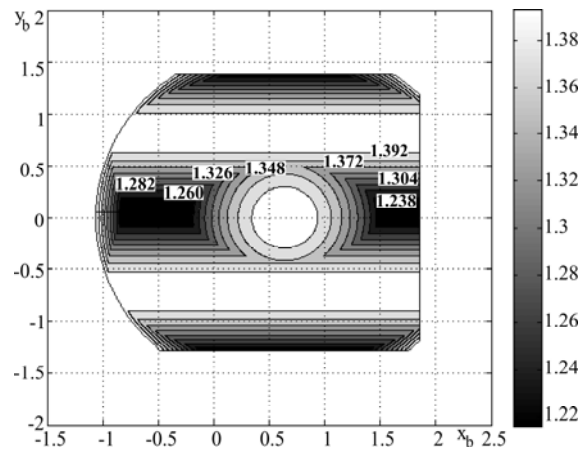
⁶ From a geometric point of view, $|s_2|$, $|s_3|$, $|s_6|$, and $|s_7|$ are equal to the distances of O_p from the lines respectively passing through O_1 and O_2 , O_2 and A_3 , O_5 and O_6 , and O_6 and A_1 ; whereas, $|s_8|$ is equal to the distance of O_p from the line parallel to k_b and passing through A_1 .



(a)

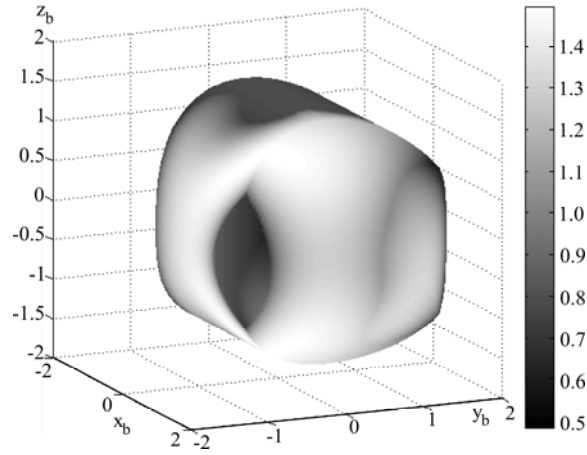


(b)

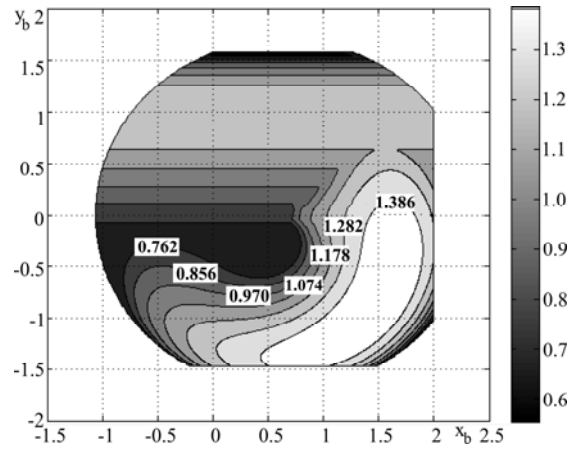


(c)

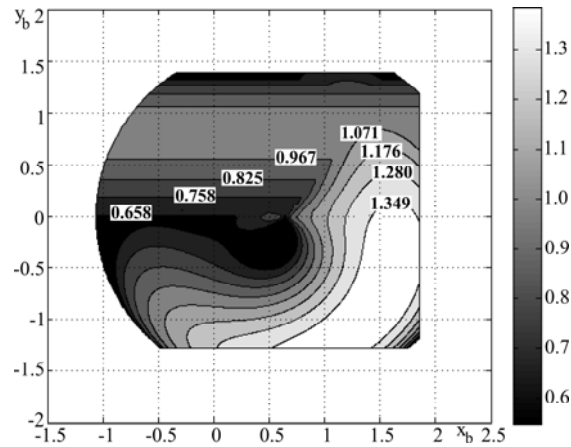
Figure 5: Values of $\delta_{g,R}$ when O_p lies (a) on the boundary surface of the workspace, (b) on the plane $z=0$, and (c) on the planes $z=\pm 0.75$ l.u. for $\theta_3 \in [0, \pi]$ and $\theta_7 \in [0, \pi]$ (the curves are the contour lines; the grayscales indicate the $\delta_{g,R}$ value).



(a)



(b)



(c)

Figure 6: Values of $\varepsilon_{g,R}$ when O_p lies (a) on the boundary surface of the workspace, (b) on the plane $z=0$, and (c) on the planes $z=\pm 0.75$ l.u. for $\theta_3 \in [0, \pi]$ and $\theta_7 \in [0, \pi]$ (the curves are the contour lines; the grayscales indicate the $\varepsilon_{g,R}$ value in [l.u./rad]).

symmetrically located with respect to the $x_b y_b$ coordinate plane [i.e., the plane $z=0$, see Fig.2(a)], the same symmetry holds for the workspace volume and, provided that only leg configurations symmetric with respect to the plane $z=0$ are considered, for the values of $\delta_{g,R}$ and $\varepsilon_{g,R}$ inside that volume, too. Leg configuration's symmetry is preserved, in the $\underline{P}RRR$ leg, by keeping either $\theta_3 \in [0, \pi]$ or $\theta_3 \in [\pi, 2\pi]$ and, in the $\underline{P}RRU$ leg, by keeping either $\theta_7 \in [0, \pi]$ or $\theta_7 \in [\pi, 2\pi]$ for any value of the z coordinate of O_p .

Figure 4 shows the workspace boundaries for a Triflex-II with the following geometric data (1.u. stands for length unit): $a_b=(20/47)$ 1.u., $a_p=(30/47)$ 1.u., $d_p=(45/94)$ 1.u., $d_s=(40/47)$ 1.u., $a_2=a_3=(40/47)$ 1.u., $a_6=a_7=(36/47)$ 1.u., $a_{11}=a_{12}=1$ 1.u.. Also, Figs. 5 and 6 show the values of $\delta_{g,R}$ and $\varepsilon_{g,R}$, respectively, computed by using the same geometric data and by keeping $\theta_3 \in [0, \pi]$ and $\theta_7 \in [0, \pi]$, when O_p lies on the boundary surface of the workspace and on the planes $z=0$ and $z=\pm 0.75$ 1.u. . Eventually, the values of $\delta_{g,R}$ and $\varepsilon_{g,R}$ have been computed with the same data inside the whole workspace and the following delimitations come out

$$1 \leq \delta_{g,R} \leq \sqrt{3} \quad (28a)$$

$$0.479 \leq \varepsilon_{g,R} \leq 1.489 \text{ (1.u./rad)} \quad (28b)$$

The introduction of the maximum computed values of $\delta_{g,R}$ and $\varepsilon_{g,R}$ into inequalities (26a) and (26b) yields:

$$|\Delta\varphi| \leq \sqrt{3} \|\Delta\mathbf{q}_{g,R}\| \quad (29a)$$

$$\|\Delta\mathbf{O}_p\| \leq \|\Delta\mathbf{q}_{f,P}\| + \sqrt{2} \|\Delta\mathbf{q}_{g,P}\| + 1.489 \|\Delta\mathbf{q}_{g,R}\| \quad (29b)$$

Thus, by choosing $|\Delta\varphi|_{\max} = 0.026180 \text{ rad} (=1.5^\circ)^7$, inequality (19a) gives the following upper bound

$$\|\Delta\mathbf{q}_{g,R}\| \leq 0.015115 \text{ rad} \quad (30)$$

Since $\|\Delta\mathbf{q}_{g,R}\|$ is equal to $\sqrt{\alpha_2^2 + \alpha_3^2 + \alpha_6^2 + \alpha_7^2 + \alpha_8^2}$, if the choice of assigning the same tolerance class, α_T , to all the angular errors $\alpha_2, \alpha_3, \alpha_6, \alpha_7$, and α_8 is adopted, inequality (30) will give the following limitation on α_T

⁷ This value of $|\Delta\varphi|_{\max}$ has been taken from the data sheets of the commercial delta robot ABB IRB-360 (<http://new.abb.com/products/robotics/industrial-robots/irb-360>).

$$\alpha_T = \frac{\|\Delta \mathbf{q}_{g,R}\|}{\sqrt{5}} \leq 0.00675965 \text{ rad} = 0^\circ 23' \quad (31)$$

Also, if $\|\Delta \mathbf{q}_{g,p}\|$ is assumed equal to 0.01(l.u.) and the joint-variable errors Δd_1 , Δd_5 , and Δd_{10} are all assumed equal to 0.0001(l.u.)⁸, $\|\Delta \mathbf{q}_{r,p}\|$ ($=\sqrt{(\Delta d_1)^2 + (\Delta d_5)^2 + (\Delta d_{10})^2}$) will be equal to 0.0001732(l.u.) and inequality (29b) will give the following upper bound

$$\|\Delta \mathbf{O}_p\| \leq 0,037 \text{ (l.u.)}$$

6. CONCLUSIONS

A general discussion on how to take into account geometric error effects has been presented. The presented discussion has brought to delineate a general method for modelling such errors and for evaluating their effects on the positioning precision in any non-overconstrained manipulator.

The presented method relies on the spectral norms of suitable Jacobians of an extended spatial mechanism (ESM) easy to deduce from the actual manipulator. Such approach overcomes the problem of the variable homogenization that arises in the methods based on the “Conditioning Index”.

Also, the introduction of the concept of “Accuracy Coefficient” makes it possible to analyze the effects both of geometric-error sets and of a single geometric error. The same concept is an effective design tool for selecting either which workspace region is less affected by geometric errors or which geometric constants must be carefully sized to reduce these effects.

The geometric errors effects in the translational parallel manipulator Triflex-II have been studied by using the proposed method.

ACKNOWLEDGMENTS

This work has been developed at the Laboratory of Advanced Mechanics (MECH-LAV) of Ferrara Technopole, supported by UNIFE funds, by Regione Emilia Romagna (District Councillorship for Productive Assets, Economic Development, Telematic Plan) POR-FESR 2007-2013, Attività I.1.1, and by CNPq –

⁸ It is worth noting that the data sheets of commercial roller-screws (see, for instance, <http://www.thomsonlinear.com/website/com/eng/index.php> or <http://www.skf.com/group/products/linear-motion/ball-and-roller-screws/roller-screws/index.html>) give $\Delta d=1\mu\text{m}$.

Conselho Nacional de Desenvolvimento Científico e Tecnológico (National Council for Scientific and Technological Development) -Project nº 232250/2014-6 - Brazil.

REFERENCES

- [1] Liu, H., Huang, T. T., and Chetwynd, D. G., 2011. “A general approach for geometric error modeling of lower mobility parallel manipulators”. *Journal of Mechanisms and Robotics*, Volume 3(Number 2), May, p. 021013.
- [2] Huang, T., Whitehouse, D. J., and Chetwynd, D. G., 2002. “A unified error model for tolerance design, assembly and error compensation of 3-dof parallel kinematic machines with parallelogram struts”. *{CIRP} Annals – Manufacturing Technology*, 51(1), pp. 297 – 301.
- [3] Di Gregorio, R., and Parenti-Castelli, V., 2002, “Geometric Errors Versus Calibration in Manipulators with Less than 6 DOF,” in: *RoManSy 14 – Theory and practice of robots and manipulators*, Bianchi G., Guinot J.-C. and Rzymkowski C. (eds.), Springer, New York, pp. 31-38.
- [4] Y. Fang and L. Tsai, “Structure synthesis of a class of 4-dof and 5-dof parallel manipulators with identical limb structures,” *The International Journal of Robotics Research*, vol. 21, no. 9, pp. 799–810, 2002.
- [5] X. Kong, C. M. Gosselin, 2007, “Type Synthesis of Parallel Mechanisms,” Springer-Verlag, Berlin Heidelberg, Germany, ISBN: 978-3-540-71989-2.
- [6] Liu, X.-J., and Wang, J., 2014. *Parallel kinematics : type, kinematics, and optimal design*. Springer tracts in mechanical engineering. Springer.
- [7] Gosselin C., and Angeles J., 1991. “A global performance index for the kinematic optimization of robotic manipulators,” *Journal of Mechanical Design*, Vol. 113, No. 3, pp. 220-226
- [8] Tian, W., Gao, W., Chang, W. and Nie, Y., 2014, “Error Modeling and Sensitivity Analysis of a Five-Axis Machine Tool”. *Mathematical Problems in Engineering*, Article ID 745250.
- [9] Merlet J-P., 2005, “Jacobian, Manipulability, Condition Number, and Accuracy of Parallel Robots”. *ASME. J. Mech. Des.*;128(1):199-206.
- [10] Li, Y., Li, C., Qu, D., Duan, S., Bai, X., and Shen, H., 2012. “Errors modeling and sensitivity analysis for a novel parallel manipulator”. In *Mechatronics and Automation (ICMA), 2012 International Conference on*, pp. 755–760.

- [11] Mei, J., Ni, Y., Li, Y., Zhang, L., and Liu, F., 2009. "The error modeling and accuracy synthesis of a 3-dof parallel robot delta-s". In Information and Automation, 2009. ICIA '09. International Conference on, pp. 289–294.
- [12] Frisoli, A., Solazzi, M., Pellegrinetti, D., and Bergamasco, M., 2011. "A new screw theory method for the estimation of position accuracy in spatial parallel manipulators with revolute joint clearances". Mechanism and Machine Theory, 46(12), pp. 1929 – 1949.
- [13] Yu, Z., Tiemin, L., and Xiaoqiang, T., 2011. "Geometric error modeling of machine tools based on screw theory". Procedia Engineering, 24, pp. 845 – 849. International Conference on Advances in Engineering 2011.
- [14] Kumaraswamy, U., Shunmugam, M., and Sujatha, S., 2013. "A unified framework for tolerance analysis of planar and spatial mechanisms using screw theory". Mechanism and Machine Theory, 69, pp. 168 – 184.
- [15] Chen, Y., Xie, F., Liu, X., and Zhou, Y., 2014. "Error modeling and sensitivity analysis of a parallel robot with scara (selective compliance assembly robot arm) motions". Chinese Journal of Mechanical Engineering, 27(4), pp. 693–702.
- [16] Angeles, J., & Rojas, A. (1987). Manipulator inverse kinematics via condition-number minimization and continuation. INT. J. ROBOTICS AUTOM., 2(2), 61-69.
- [17] Campos, A. A., Guenther, R., and Martins, D., 2009. "Differential kinematics of parallel manipulators using Assur virtual chains". Proceedings of the Institution of Mechanical Engineers. Part C, Journal of Mechanical Engineering Science, 223, pp. 1697–1711.
- [18] Davies, T. H., 1981. "Kirchhoff's circulation law applied to multi-loop kinematic chain". Mechanism and Machine Theory, 16, pp. 171–173.
- [19] Tsai, L.-W., 1999, "Robot Analysis: the Mechanics of serial and parallel manipulators," John Wiley & Sons, New York.
- [20] Hervé J.M., 1994, "The mathematical group structure of the set of displacements," Mechanism and Machine Theory, Vol. 29, No. 1, pp. 73-81.
- [21] Meyer C. D., 2000, "Matrix Analysis and Applied Linear Algebra," Society for Industrial & Applied Mathematics (SIAM).
- [22] Gosselin, C.M., and Angeles, J., 1990, "Singularity analysis of closed-loop kinematic chains," IEEE Transactions on Robotics and Automation, Vol. 6 (1990), No. 3, pp. 281-290.

- [23] Ma, O., and Angeles, J., 1991, "Architecture singularities of platform manipulators," Proc. of the 1991 IEEE Int. Conf. on Robotics and Automation, Sacramento (CA, USA), pp. 1542-1547.
- [24] Zlatanov, D., Fenton, R.G, and Benhabib, B., 1995, "A unifying framework for classification and interpretation of mechanism singularities," ASME J. of Mechanical Design, Vol. 117 (1995), No. 4, pp. 566-572.
- [25] Simas, H., Martins, D. and Simoni, R., 2013. "Uma Classe de Manipuladores Paralelos de Configuração Variável com Autoalinhamento," Patent: BR1020130267716, INPI - Instituto Nacional da Propriedade Industrial - Brazil.
- [26] Simoni, R., Simas, H. and Martins, D., 2014. "TRIFLEX: Design and Prototyping of a 3-DOF Variable-Configuration Parallel Manipulator with Self-Aligning," International Journal of Mechanical Engineering and Automation, **1**, pp. 77-82.
- [27] Simoni, R., Simas, H., and Martins, D. ,2013. "Uma Classe de Manipuladores Paralelos de Configuração Variável". Patent: BR102013026774, INPI - Instituto Nacional da Propriedade Industrial - Brazil.
- [28] Gosselin, C. M. Gosselin, Kong, X., Foucault, S. and Bonev, I. A., 2004. "A Fully Decoupled 3-DOF Translational Parallel Mechanism," *Proc. of the 4th Chemnitz Parallel Kinematics Seminar; Parallel Kinematic Machines International Conference*, Chemnitz: Germany, pp. 595-610.
- [29] Lecours, A., and Gosselin, C., 2009. "Determination of the workspace of a 3-prpr parallel mechanism for human-robot collaboration". Transactions of the Canadian Society for Mechanical Engineering, **33**(4), pp. 609-618.
- [30] Klimchik, A., Chablat, D.,and Pashkevich, A, 2014. "Stiffness modeling for perfect and non-perfect parallel manipulators under internal and external loadings." Mechanism and Machine Theory, **79**, pp.1-28.
- [31] Caro, S., Wenger, P., Bennis, F., and Chablat, D, 2006. "Sensitivity Analysis of the Orthoglide, a 3-DOF Translational Parallel Kinematic Machine." ASME Journal of Mechanical Design, **128**, pp.392-402.

FIGURE CAPTIONS

Figure 1: Graph of a manipulator with general architecture: vertices and arcs represent links and joints, respectively; L_i for $i=1, \dots, n$ are open kinematic chains (legs) which simultaneously connect the platform to the base; whereas, L_t is an added virtual kinematic chain.

Figure 2: Triflex-II: (a) kinematic scheme, and (b) platform's reference points.

Figure 3: Introduction of the geometric errors: (a) $\underline{P}RRU$ and (b) $\underline{P}RRR$ legs with geometric errors.

Figure 4: Workspace boundaries: (a) intersection with the $x_b y_b$ -plane, (b) intersection with the $y_b z_b$ -plane, (c) intersection with the $x_b z_b$ -plane, and (d) 3D view (the grayscale indicates the z_b value in [l.u.]).

Figure 5: Values of $\delta_{g,R}$ when O_p lies (a) on the boundary surface of the workspace, (b) on the plane $z=0$, and (c) on the planes $z= \pm 0.75$ l.u. for $\theta_3 \in [0, \pi]$ and $\theta_7 \in [0, \pi]$ (the curves are the contour lines; the grayscales indicate the $\delta_{g,R}$ value).

Figure 6: Values of $\varepsilon_{g,R}$ when O_p lies (a) on the boundary surface of the workspace, (b) on the plane $z=0$, and (c) on the planes $z= \pm 0.75$ l.u. for $\theta_3 \in [0, \pi]$ and $\theta_7 \in [0, \pi]$ (the curves are the contour lines; the grayscales indicate the $\varepsilon_{g,R}$ value in [l.u./rad]).

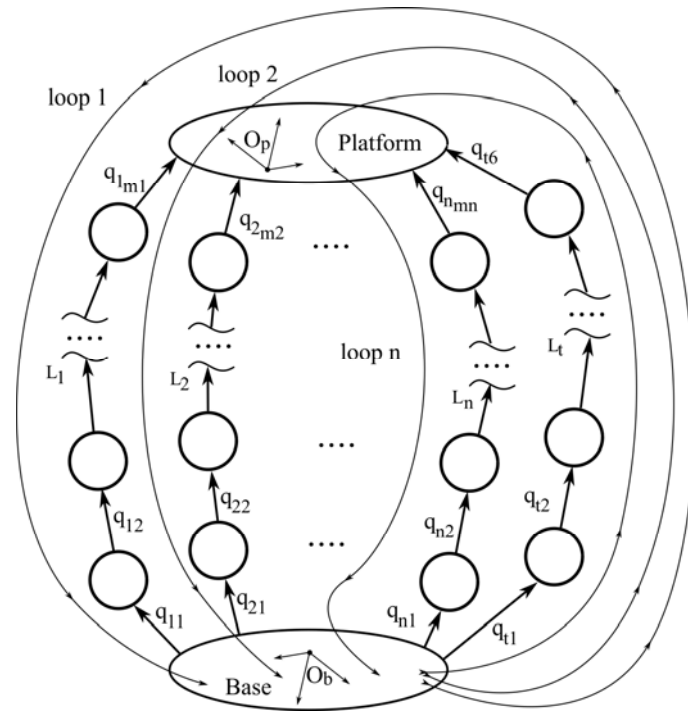
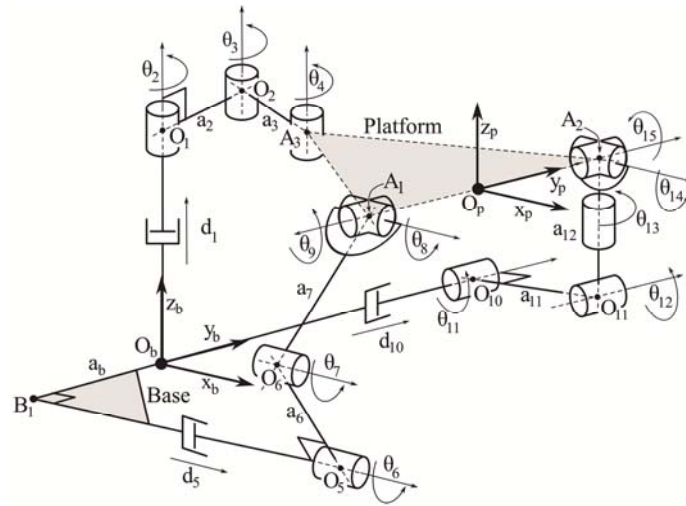
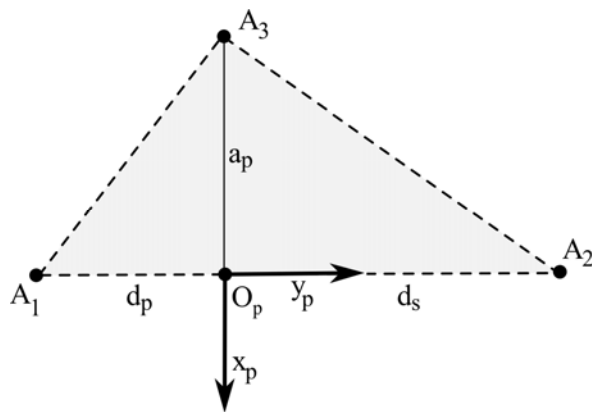


Figure 1: Graph of a manipulator with general architecture: vertices and arcs represent links and joints, respectively; L_i for $i=1, \dots, n$ are open kinematic chains (legs) which simultaneously connect the platform to the base; whereas, L_t is an added virtual kinematic chain.



(a)



(b)

Figure 2: Triflex-II: (a) kinematic scheme, and (b) platform's reference points.

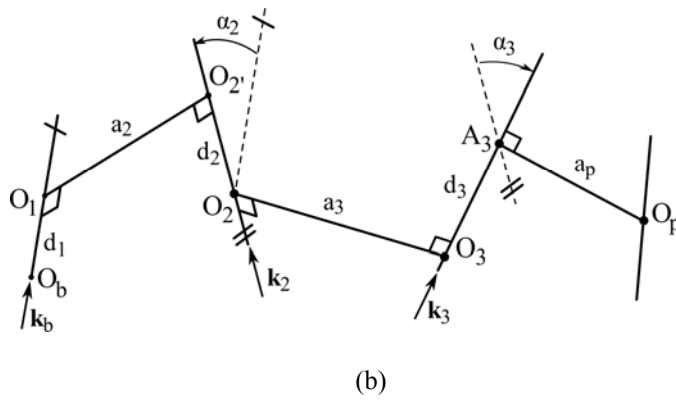
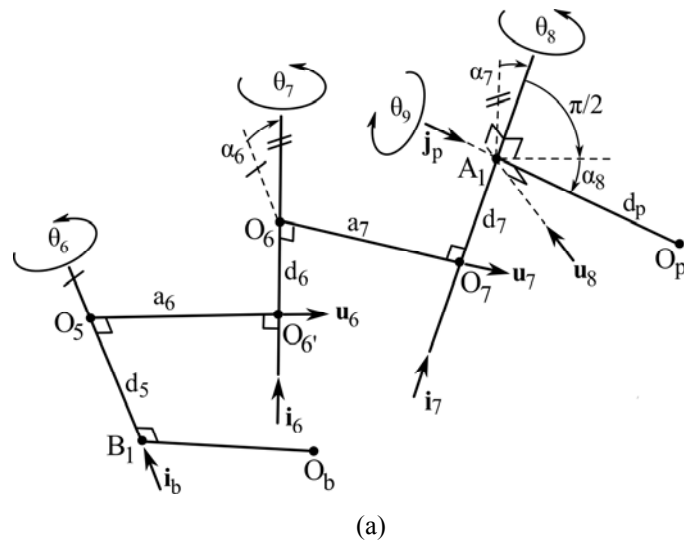


Figure 3: Introduction of the geometric errors: (a) PRRU and (b) PRRR legs with geometric errors.

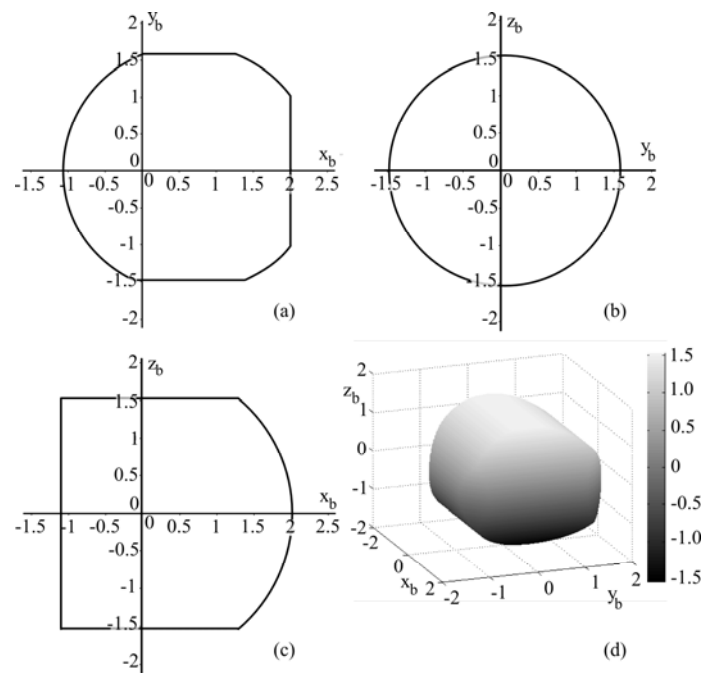
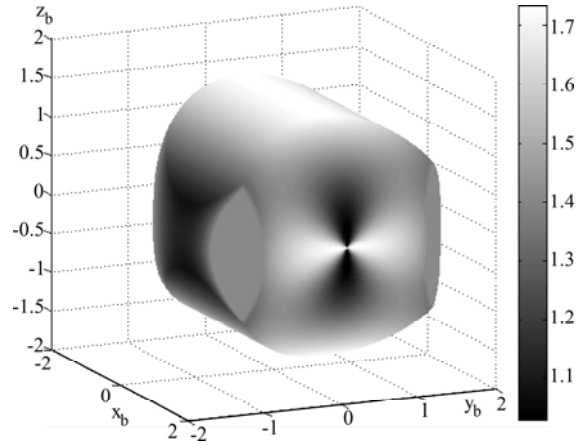
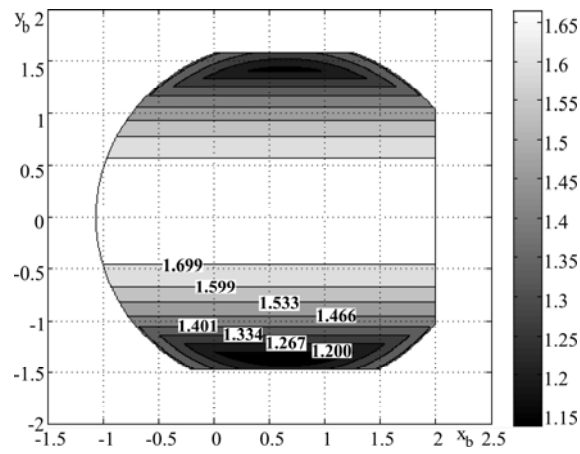


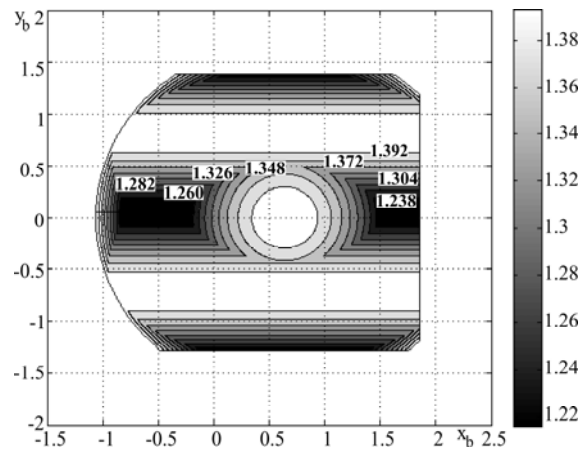
Figure 4: Workspace boundaries: (a) intersection with the $x_b y_b$ -plane, (b) intersection with the $y_b z_b$ -plane, (c) intersection with the $x_b z_b$ -plane, and (d) 3D view (the grayscale indicates the z_b value in [l.u.]).



(a)

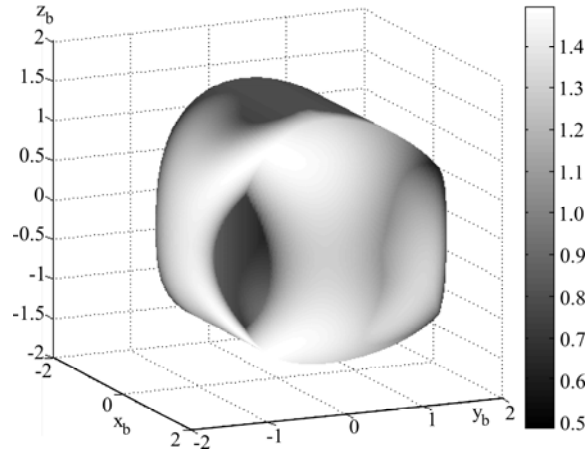


(b)

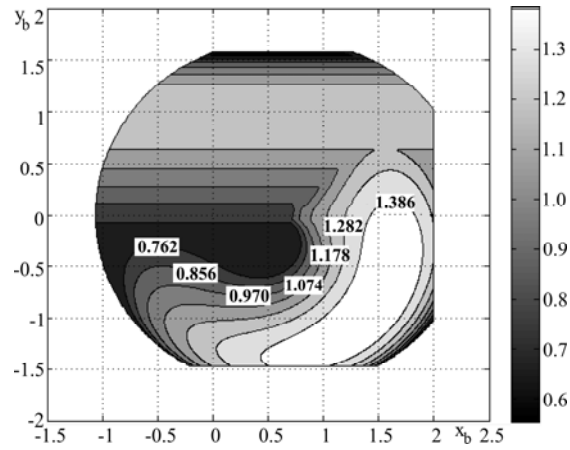


(c)

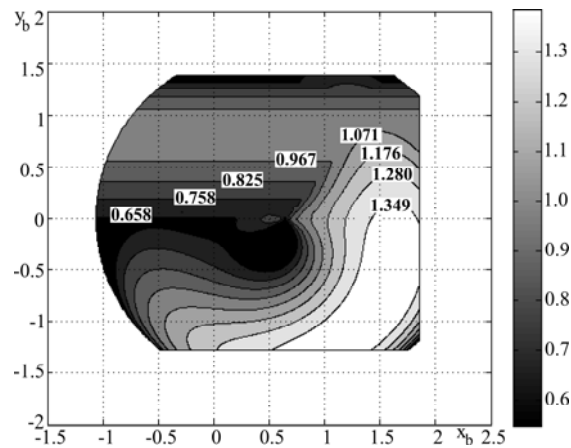
Figure 5: Values of $\delta_{g,R}$ when O_p lies (a) on the boundary surface of the workspace, (b) on the plane $z=0$, and (c) on the planes $z=\pm 0.75$ l.u. for $\theta_3 \in [0, \pi]$ and $\theta_7 \in [0, \pi]$ (the curves are the contour lines; the grayscales indicate the $\delta_{g,R}$ value).



(a)



(b)



(c)

Figure 6: Values of $\varepsilon_{g,R}$ when O_p lies (a) on the boundary surface of the workspace, (b) on the plane $z=0$, and (c) on the planes $z=\pm 0.75$ l.u. for $\theta_3 \in [0, \pi]$ and $\theta_7 \in [0, \pi]$ (the curves are the contour lines; the grayscales indicate the $\varepsilon_{g,R}$ value in [l.u./rad]).